Velocity-independent τ-p moveout in a horizontally-layered VTI medium [a]

[a]Published in Geophysics, 76, no. 4, U45-U57, (2011)

Lorenzo Casasanta and Sergey Fomel

ABSTRACT

Local slopes of seismic events carry complete information about the structure of the subsurface. This information is sufficient for accomplishing all time-domain imaging tasks, without the need to estimate or know the seismic velocity model. We develop a velocity-independent τ-p imaging approach to perform moveout correction in horizontally-layered VTI media. The effective and interval anisotropic parameters turn into data attributes through the use of slopes and become directly mappable to the zero-slope traveltime. The τ-p transform is the natural domain for anisotropy parameter estimation in layered media, because the phase velocity is given explicitly in terms of p. Therefore, the τ-p transform allows for reflection-traveltime modeling and inversion that are simpler than traditional methods based on Taylor-series expansions of traveltime in t-X domain. Synthetic and field data tests demonstrate the practical effectiveness of our method.

INTRODUCTION

macro model of the subsurface and remains one of the most labor-intensive and time-consuming procedures in the conventional approach to seismic data analysis (Yilmaz, 2000). In time-domain imaging, effective seismic velocities are picked from coherency scans. Moreover, anisotropic velocity model building requires more than just a single parameter scan for nonhyperbolic traveltime approximation (Alkhalifah and Tsvankin, 1995). This means that anisotropic velocity analysis is at least twice more computationally intensive than its traditional isotropic counterpart. Conventional human-aided velocity analysis takes up a significant part of the time needed to process seismic data. Even with semi-automatic picking software, this phase alone might take weeks or even months for modern 3D data sets. Several approaches have been proposed to automatize and simplify velocity analysis and traveltime picking procedures in order to reduce the time and manual work required for handpicked velocities (Lambaré, 2008; Lambaré et al., 2003; Siliqi et al., 2007). However, these tools still require significant manual inspection and editing for quality control.

The idea of using local event slopes estimated from prestack seismic data goes back to the work of Rieber (1936) and Riabinkin (1957). Several following papers

outline the importance of local data slopes in seismic data processing, particularly the role that slope estimates play in the algorithm of stereotomography (Sword, 1987; Lambaré, 2008; Lambaré et al., 2003). The concept of velocity-independent time-domain imaging goes back to Ottolini (1983). Wolf et al. (2004) pointed out that it is possible to perform hyperbolic moveout velocity-analysis by estimating local data slopes in the prestack data domain using an automated method such as plane-wave destruction (Fomel, 2002). This methodology is attractive because it can be less time-consuming than the manual work required to handpick velocities.

By estimating local event slopes in prestack seismic reflection data, Fomel (2007b) demonstrated that it is possible to accomplish all common time-domain imaging tasks, from normal moveout to prestack time migration, without the need to estimate seismic velocities or other attributes. Local slopes contain complete information about the reflection geometry. Once they are estimated, seismic velocities and all the other moveout parameters turn into data attributes and become directly mappable from the prestack data domain into the time-migrated image domain. Fomel (2007b) focused on the isotropic prestack time processing and showed several results of oriented (slope-based) velocity analysis and imaging, both on synthetic and real data. Although he developed the mathematical framework for velocity-independent non-hyperbolic processing in the time-offset t-X domain, he did not provide examples to demonstrate its use and efficacy. Burnett and Fomel (2009a,b) extended the method to 3D elliptically anisotropic moveout corrections.

In this paper, we extend the concept of velocity-independent seismic processing to P-wave VTI data in the τ-p or slant-stack domain obtained by Radon-transforming CMP data. We account for VTI anisotropy only, but the theory developed here should work for a general anisotropic horizontally-layered velocity model. We assume that each layer is laterally homogeneous with a horizontal symmetry plane and that the incidence plane represents a symmetry plane for the model as a whole so that wave propagation is two-dimensional. The τ-p transform is the natural domain for anisotropic parameter estimation in layered media (van der Baan and Kendall, 2002; Douma and van der Baan, 2008; Fomel, 2008) because it allows for simpler and more accurate moveout modeling and inversion than the conventional methods applied in t-X domain. Since the horizontal slowness is preserved, each trace in τ-p CMP gathers sees the contributions of rays that share the same segments of trajectory in the layers. Therefore, one can simply sum the contribution of each individual layer and obtain the overall τ-p moveout signature. This makes modelling or ray tracing a linear procedure. Moreover, by literally subtracting all the unwanted layers, we can isolate the contribution of a specific layer and access directly its interval parameters without relying on the effective-parameter approximations as normally happens in t-X domain.

After τ-p transform, seismic data are mapped to the slowness domain, where the reflection signature depends on the vertical component of phase slowness. Phase velocity is the natural parameter to work with in the case of anisotropic data, because explicit expressions exist for phase velocities in all the anisotropic media that display

an horizontal symmetry plane. Unfortunately, exact expressions for τ-p signatures are not always practical. Nevertheless, approximate expressions provide accurate traveltime predictions (Tsvankin et al., 2010).

After describing the advantages of processing anisotropic data in the τ-p domain, we derive the oriented (slope-based) NMO equation that describes direct mapping from prestack data to zero-slope time (analogous to zero-offset time in t-X domain). We obtain the effective values of anisotropy parameters as data attributes derived from local slope and curvature estimates and directly mappable to the appropriate zero-slope time. Similarly to conventional t-X processing, several procedures applied in τ-p domain rely on coherency analysis (van der Baan and Kendall, 2002; Sil and Sen, 2008) or traveltime picking plus inversion (Wang and Tsvankin, 2009; Fowler et al., 2008) to retrieve the anisotropy parameters. We believe that our procedure is more attractive because it is fully automated and less time-consuming than searching for the best-fit moveout trajectory through simultaneous two-parameter inversion or semblance scans.

Interval parameters as well as effective parameters can be regarded as data attributes obtained from local slopes. Unlike t-X domain, processing data in τ-p offers two alternatives to conventional Dix (1955) inversion: *stripping* and *Fowler's equations* (Fowler et al., 2008). These relations can be considered as the VTI extension of the "straightedge determination of interval velocity" method proposed by Claerbout (1978). These three formulations for interval-parameter inversion require an estimate of the local-curvature field. To estimate curvature, we perform a numerical differentiation of the slope estimates. This procedure usually returns noisy and biased curvature values that affect parameter estimation, especially for those parameters that control long-spread/large-angle moveout.

Fowler's equations offer a solution to this problem. In these equations, the curvature dependence is absorbed by the zero-slope time that we can estimate by applying the predictive painting algorithm (Fomel, 2010). This approach does not involve any curvature estimation and represents a more robust way for obtaining the zero-slope time mapping field required (1) to automatically flatten or NMO correct the τ-p CMP gathers (2) to retrieve interval parameters using the curvature-independent Fowler's equations. This last approach to data processing makes the anisotropy-parameter estimation closer to an imaging processing task. Its only requirement is the ability to extract the best local-slope field from the data.

THE τ-p DOMAIN

The τ-p transform is the natural domain for anisotropy parameters estimation in layered or vertically varying media with horizontal symmetry planes (van der Baan and Kendall, 2002; Douma and van der Baan, 2008; Sil and Sen, 2008; Tsvankin et al., 2010). Since the horizontal slowness is preserved upon propagation, the τ-p transform allows simpler and more accurate traveltime modeling (ray tracing) and

inversion (layer stripping). Moreover, the τ-p transform is a plane-wave decomposition. Therefore, the phase velocity, rather than the group velocity, is the relevant velocity. The group velocity controls instead traveltime in the traditional t-X domain (Tsvankin, 2006). Unfortunately, the exact expressions for the group velocities in terms of the group angle are difficult to obtain and cumbersome for practical use. As a result, it requires either ray tracing for exact t-X modeling in anisotropic media or the use of multi-parameter traveltime approximations. In this domain, the most straightforward and widely used approximation for P-waves reflection moveout comes from the Taylor series expansion of traveltime or squared traveltime around the zero offset (Taner and Koehler, 1969; Ursin and Stovas, 2006):

$$t^k(x) = \sum_{n=0}^{N} A_{2n}\, x^{2n} \quad \text{with} \quad k = 1, 2 \tag{1}$$

Although it is possible to derive exact formulas for all the series coefficients (Al-Dajani and Tsvankin, 1998; Tsvankin, 1995, 2006), equation 1 loses its accuracy with increasing offset to depth ratio. Fomel and Stovas (2010) introduced recently a generalized functional form for approximating reflection moveout at large offsets. While the classic Alkhalifah and Tsvankin (1995) 4th-order Taylor/Padé approximation uses three parameters, the generalized approximation involves five parameters, which can be determined from the zero-offset computation and from tracing one nonzero-offset ray. In a homogeneous quasi-acoustic VTI medium (Alkhalifah, 1998), the generalized approximation of Fomel and Stovas (2010) reduces to the three-term traveltime approximation of Fomel (2004), which is practical and more accurate than other known three-parameter formulas for non-hyperbolic moveout.

The τ-p domain provides an attractive alternative to computing P-wave reflection-moveout curves. The τ-p transform stacks the data gathered in t-X domain along straight lines, whose direction

$$t \;=\; \tau \;+\; p\, X, \tag{2}$$

is parametrized by the horizontal slowness p and the intercept time τ (blue lines in figure 1a). Hence, the τ-p transform maps the data to the slowness domain, where traveltime depends on the vertical components q of the down and upgoing phase slowness [equation 20 in van der Baan and Kendall (2002)]. Considering an anisotropic medium with a horizontal symmetry plane (VTI, HTI and orthorhombic with one of the symmetry axis aligned to the depth direction), the τ-p reflection moveout formula simplifies to

$$\tau(p) = \tau_0\, V_{P0}\, q(p)\ , \tag{3}$$

where $\tau_0 = \frac{2z}{V_{P0}}$ is the zero-slope/zero-offset two way traveltime in a homogeneous layer with thickness z and vertical velocity V_{P0}. According to the Christoffel equation, $q(p) = \sqrt{1/v^2(p) \;-\; p^2}$ and $v = v(p)$ is the phase velocity as a function of the ray parameter p.

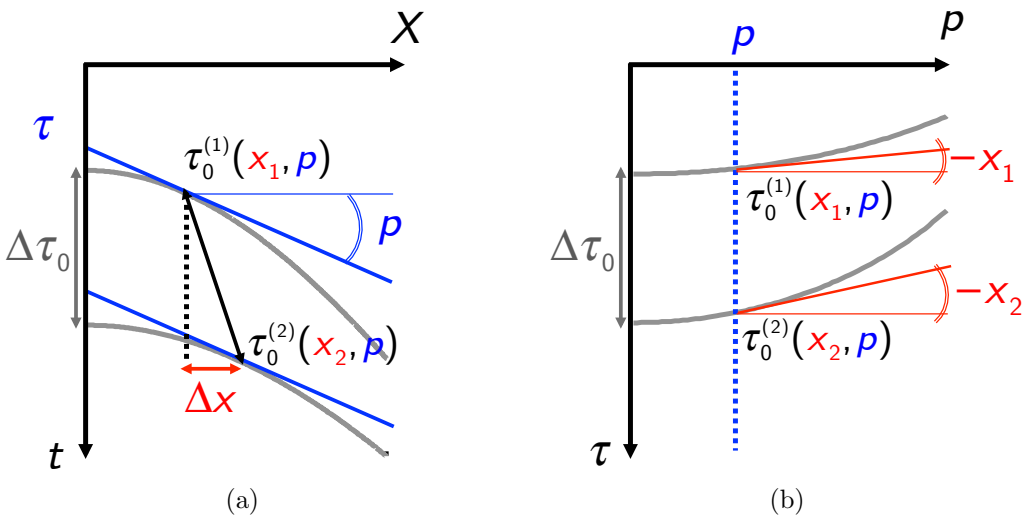

Figure 1: Comparison between event geometry in t-X (a) and τ-p (b). The τ-p domain naturally unveils the position of equal slope events. If the medium is a stack of horizontal homogeneous layers, a τ-p trace collects the contribution of rays, with ray parameter p, that share common ray segments in each layer. Moreover, local slopes $R = \frac{d\tau}{dp}$ are related to emerging offset $x = -R$. After the original t-X data is τ-p transformed, we can measure zero-slope traveltime $\Delta\tau_0 = \frac{\partial\tau_0}{\partial\tau}\Delta\tau$ and offset $\Delta x = -\frac{\partial R}{\partial\tau}\Delta\tau$ differences at common slope p points, by simple differentiation along τ.

Equation 3 remains exact as long as we use the exact expression for the phase velocity $v(p)$ (red solid line in figure 2a). Exact expressions exist for all types of anisotropic media with a horizontal symmetry plane. Unfortunately, the exact and the highly accurate (Stovas and Fomel, 2010) expressions for τ-p signatures are not very practical because they depend on multiple parameters. In practice, one may prefer to employ three-parameters approximate relations for the phase velocity. Although these signatures are approximate, they are more reliable then the τ-p transformed version of their dual-pair in the t-X domain (figure 2b).

We can extend the result in equation 3 to a stack of N horizontal homogeneous layers with horizontal symmetry planes. According to Snell's law, the horizontal slowness p is preserved upon propagation through each layer. Thus, the total intercept time τ from the bottom of N-th layer is the summation of each interval intercept time $\Delta\tau_n$ in the N contributing layers:

$$\tau(p) = \sum_{n=1}^{N} \Delta\tau_n = \sum_{n=1}^{N} V_{P0,n}\; q_n(p)\; \Delta\tau_{0,n} \quad , \tag{4}$$

where each single intercept time $\Delta\tau_n$ obviously depends just on interval parameters characterizing the n-th layer. Equation 4 states that in the τ-p domain both the ray tracing (forward modeling) and layer stripping (inversion) are linear processes. Each trace in a τ-p gather collects the contribution of rays that share common segments of trajectory in the layers (Figure 1a). Moreover, the τ-p domain helps us also to isolate

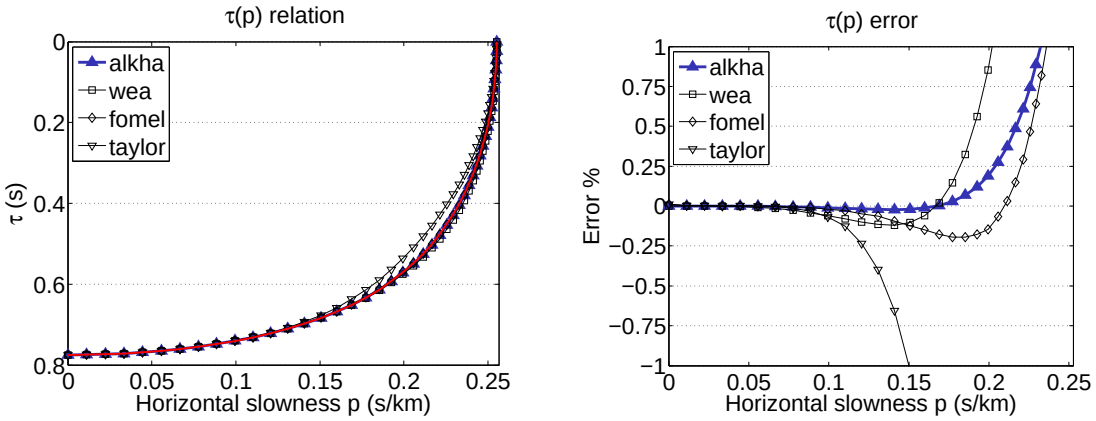

(a) (b)

Figure 2: (a) $\tau(p)$ signatures: Thomsen (1986) or Byun et al. (1989) weak anisotropy (squares) and Alkhalifah (2000) quasi-acoustic (blue upper triangles) approximation. (b) percentage error with respect to the exact formulation (red solid line). These curves are computed in a layer of 1.24 km thickness with $V_{P0} = 3.2$ km/s, $V_N = 2.9$ km/s, $V_H = 3.9$ km/s, η=0.44 and $V_{P0}/V_{S0} = 2.5$. The Taylor curve (lower triangles) represent the τ-p transformed quartic moveout traveltime approximation described in Alkhalifah and Tsvankin (1995). The Fomel curve (diamonds) is the τ-p mirror of the t-X moveout formula based on the shifted hyperbola approximation for the group velocity introduced by Fomel (2004).

the effect of a single layer, thereby producing an estimate for its interval properties. Layer stripping is self-explanatory: by literally subtracting all the unwanted layers, one can isolate the contribution of a specific layer and access directly its interval parameters without passing through the effective parameters as normally happens in t-X domain. In t-X processing, the traveltime curves are inverted using a two-step procedures. First, effective parameters are obtained by semblance scans. Next, interval parameters are obtained using the Dix formula or layer-stripping procedures. The τ-p processing offers instead a direct access to interval parameters.

The summation in equation 4 can be substituted by a convenient relation in term of the effective parameters obtained from the Dix average of interval ones. This result will be used in the next section to derive a closed-form expression for P-waves τ-p reflection moveout in terms of interval or effective normal-moveout velocity V_N and horizontal velocity V_H (or, alternatively, η): these two parameters control all time-domain processing steps in VTI media (Alkhalifah and Tsvankin, 1995).

VELOCITY INDEPENDENT τ-P MOVEOUT IN VTI

Under the quasi-acoustic approximation (Alkhalifah, 1998, 2000) in a VTI homogeneous layer, the vertical slowness q can be expressed as a function of the horizontal

slowness p:

$$q(p) = \frac{1}{\hat{V}_{P0}} \sqrt{\frac{1 - \hat{V}_H^2 p^2}{1 - [\hat{V}_H^2 - \hat{V}_N^2] p^2}}, \tag{5}$$

where $\hat{V}_H$ and $\hat{V}_N$ are the horizontal and normal moveout velocity in the layer. In the following equations, the hat superscript ($\hat{}$) indicates layer or interval parameters. Considering a stack of N horizontal homogeneous layers with horizontal symmetry planes, we can insert equation 5 into equation 4 to obtain an expression for the τ-p reflection time from the bottom of the N-th layer, as follows:

$$\tau(p) = \sum\nolimits_{n=1}^{N} \sqrt{\frac{1 - \hat{V}_{H,n}^2 p^2}{1 - [\hat{V}_{H,n}^2 - \hat{V}_{N,n}^2] p^2}} \Delta\tau_{0,n} \tag{6}$$

where $\Delta\tau_{0,n}$ is the two way vertical time for the n-th layer. To simplify the following theoretical derivations, we assume that, instead of having a layered velocity model, interval parameters are vertically-varying continuous profiles. Therefore, we replace the summation in formula 6 with an integral along the vertical time τ_0 and arrive at the following τ-p moveout formula for a vertically-heterogeneous VTI medium:

$$\tau(p) = \int_0^{\tau_0} \sqrt{\frac{1 - \hat{V}_H^2(\xi) p^2}{1 - [\hat{V}_H^2(\xi) - \hat{V}_N^2(\xi)] p^2}} d\xi, \tag{7}$$

where $\hat{V}_N = \hat{V}_N(\xi)$ and $\hat{V}_H = \hat{V}_H(\xi)$ are (smooth) functions for interval NMO and horizontal velocities, and τ_0 is the vertical time. The vertical heterogeneity is measured as a function of τ_0. The anellipticity parameter $\hat{\eta} = \frac{1}{2}\left(\frac{\hat{V}_H^2}{\hat{V}_N^2} - 1\right)$ is also a function of the vertical time τ_0. Using effective parameters, equation 7 can be approximated by

$$\tau(p) \approx \tau_0 \sqrt{\frac{1 - V_H^2(\tau_0) p^2}{1 - [V_H^2(\tau_0) - V_N^2(\tau_0)] p^2}}, \tag{8}$$

where the effective NMO V_N and horizontal V_H velocity are related to the interval parameters through the second- and fourth-order average velocities (Taner and Koehler, 1969; Ursin and Stovas, 2006) by the following direct Dix-type formulas:

$$V_N^2(\tau_0) = \frac{1}{\tau_0} \int_0^{\tau_0} \hat{V}_N^2(\xi) d\xi, \tag{9}$$

$$S(\tau_0) V_N^4(\tau_0) = \frac{1}{\tau_0} \int_0^{\tau_0} \hat{S}(\xi) \hat{V}_N^4(\xi) d\xi, \tag{10}$$

where S is the ratio between the fourth- and second-order moments or the heterogeneity factor (de Bazelaire, 1988; Alkhalifah, 1997; Siliqi and Bousquié, 2000).

Equation 8 is basically the four-parameters rational approximation defined in τ-p domain Stovas and Fomel (2010)

$$\tau(p) \approx \tau_0 \sqrt{1 - V_N^2 p^2 + \frac{A\, V_N^4\, p^4}{1 - B\, V_N^2\, p^2}}, \tag{11}$$

with parameter $A = (1-S)/4$ defined from the Taylor series expansion of the exact τ-p function (Ursin and Stovas, 2006). Under the acoustic VTI approximation, $B = -A$ and the equation 11 now depends on three parameters only. Finally, to be consistent with equation 8, the heterogeneity coefficient becomes $S = 4\dfrac{V_H^2}{V_N^2} - 3$. In principle, it is possible to use any other three-parameters approximation in τ-p domain apart from the rational approximation 11 like, for example, the shifted ellipse approximation given by Stovas and Fomel (2010). The reason for choosing the approximation 8 is that it accurately describes the τ-p moveout for a single VTI layer (blue line in figure 2b). Nevertheless, approximation 8 remains valid for vertically heterogeneous VTI media with a decrease in accuracy for larger angles (large values of p) because of the Dix averaging

Letting R represent the slope $\tau'(p)$ and Q the curvature $\tau''(p)$, we differentiate equation 8 once

$$R(\tau, p) = -\frac{\tau(V_H^2 - Y)p}{(1 - p^2 Y)\,(1 - p^2 V_H^2)}, \tag{12}$$

and twice

$$Q(\tau, p) = -\frac{\tau F(p)(V_H^2 - Y)}{(1 - p^2 Y)^2\,(1 - p^2 V_H^2)^2}, \tag{13}$$

where $F(p) = 1 + 2p^2 Y - 3p^4 V_H^2 Y$ with $Y = V_H^2 - V_N^2$. Equations 12 and 13 provide an analytical description of the slope and curvature fields for given effective values V_N and V_H. Here we have omitted the τ_0 dependency for clarity in the notation. Since τ-p and t-X domains are mapped by the linear transformation in equation 2, we observe that

$$\tau'(p) = R = -x. \tag{14}$$

Thus, the negative of the slope R has the physical meaning of emerging offset, as pointed out by van der Baan (2004). Moreover, when the curvature Q changes sign, there is an inflection point in the τ-p wavefront that is as a condition for caustics in t-X domain. (Roganov and Stovas, 2011).

Given slope R and curvature Q fields in a τ-p CMP gather, we can eliminate the velocity V_N and the parameter Y in equations 12 and 13, thus obtaining a "velocity-independent" (Fomel, 2007b) moveout equation in the τ-p domain:

$$\tau_0(\tau, p) = \tau \sqrt{\frac{\tau p Q + 3\tau R - 3pR^2}{\tau p Q + 3\tau R + pR^2}}. \tag{15}$$

Equation 15 describes a direct mapping from events in the prestack τ-p data domain to zero-slope time τ_0. This equation represents the oriented or slope-based

moveout correction. As follows from equations 12 and 13, the effective parameters, if needed for other tasks, are given by the following relations as a function of the slope and curvature estimates (see Table 1):

$$V_N^2(\tau,p) = -\frac{1}{p}\frac{16\tau R^3}{ND}, \tag{16}$$

$$V_H^2(\tau,p) = \frac{1}{p^2}\frac{N-4\tau R}{N}, \tag{17}$$

and

$$\eta(\tau,p) = \frac{1}{p}\frac{N(4\tau R - D)}{32\tau R^3}. \tag{18}$$

In the above equations, $N = \tau pQ + 3\tau R - 3pR^2$ and $D = \tau pQ + 3\tau R + pR^2$ represent the terms in the numerator N and denominator D of the square root in equation 15. In the isotropic or elliptically anisotropic case ($V_N = V_H$ or $\eta = 0$), equations 15 to 18 simplify to equations

$$\tau_0(\tau,p) = \sqrt{\tau^2 - \tau pR} \tag{19}$$

and

$$V_N^2(\tau,p) = \frac{R}{p(pR-\tau)}\ , \tag{20}$$

previously published by Fomel (2007b).

The anisotropic parameters V_N and V_H (or η) are no longer a requirement for the moveout correction, as in the case of conventional NMO processing, but rather they are data attributes derived from local slopes and curvatures. Moreover, these parameters are mappable directly to the appropriate zero-slope time τ_0, according to equation 15.

SYNTHETIC EXAMPLE OF EFFECTIVE-PARAMETER ESTIMATION

We first test our method on a synthetic example, where the exact velocity model is known. The example is introduced in Figure 3. The synthetic data were generated by applying inverse τ-p NMO with time-variable effective velocities. Both the effective NMO V_N and horizontal V_H velocity increase linearly with vertical time and include a sinusoidal change with time, as described by the following relations

$$V_N(\tau_0) = 2.0 + 0.03\sin(2\pi\frac{\tau_0}{2}) + 0.08\tau_0,$$

$$V_H(\tau_0) = 2.2 - 0.02\sin(2\pi\frac{\tau_0}{3}) + 0.05\tau_0.$$

The CMP maximum offset-to-depth ratio is nearly 2.0 for large value of the horizontal slope p. This should guarantee the necessary data sensitivity for resolving high-order moveout parameters (Tsvankin, 2006). Figure 3b shows local event slopes

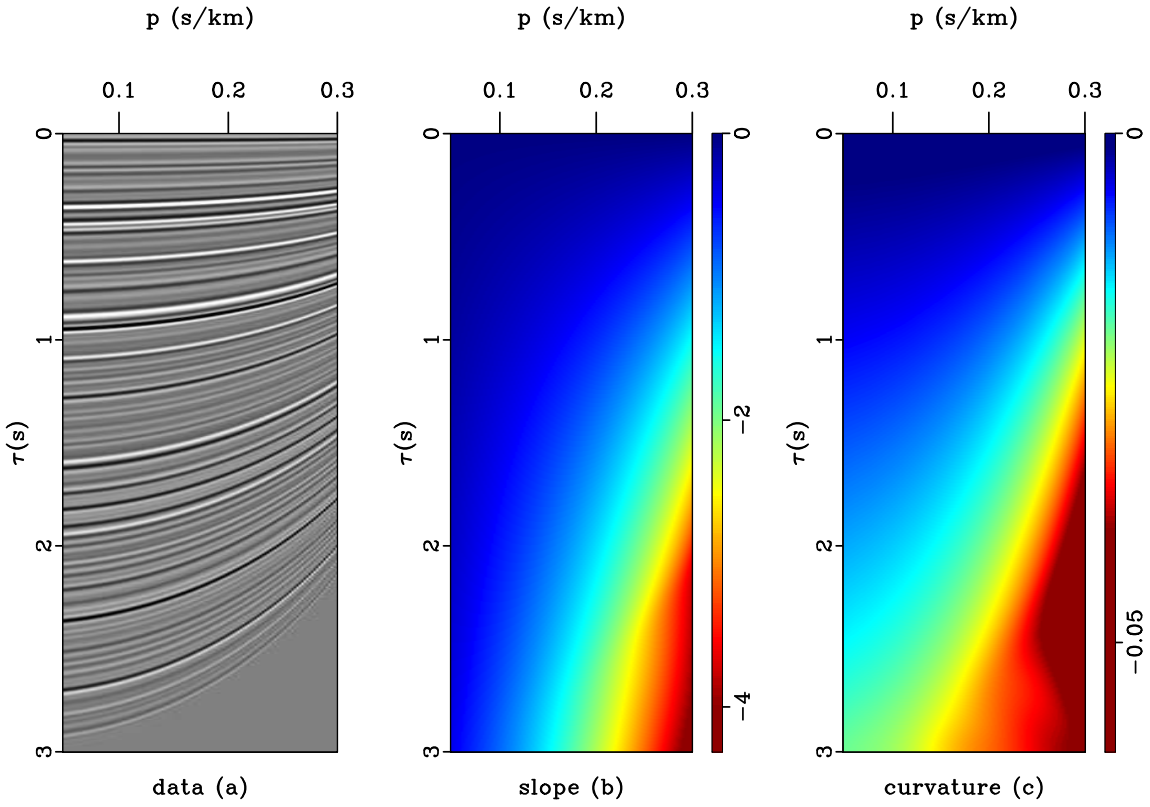

Figure 3: (a) A synthetic τ-p CMP gather composed of non elliptical events modeled using equation 8. Estimated local slopes (b) and curvatures (c).

R measured from the data using the plane-wave destruction (PWD) algorithm (see Appendix A). Plane-wave destruction predicts each seismic trace from a neighboring one along local slopes. As explained in appendix A, local slopes are extracted by minimizing the prediction error in an iterative regularized least-squares optimization. Shaping regularization controls the smoothness of the estimated slope field (Fomel, 2007a). If the seismic data are particularly noisy, a more aggressive regularization can help in getting a more consistent and stable estimate. For cleaner data, less smoothing yields a better-resolved and detailed slope field.

Unlike slopes, we don't directly estimate the curvature field Q. We compute the curvature by simply differentiating the slope estimate. Since slope $R = R(\tau, p)$ depends on both the current ray parameter p and the time $\tau = \tau(p)$, which is again a function of p, we compute the derivative of the slope field by a straightforward application of the chain rule, as follows:

$$Q = \frac{\partial R}{\partial p} + R\,\frac{\partial R}{\partial \tau}, \tag{21}$$

The slope gradient components are easily obtained by numerical differentiation. Unfortunately, this procedure suffers from numerical instability, because finite differences act like a high-pass filter that enhances the high frequency noise, especially when we are dealing with real data set with poor SNR (signal-to-noise ratio). A noisy or biased estimate of the curvature field may affect the final result. Figure 3c shows the curvature field Q for the synthetic data, computed according to equation 21.

Figure 4b represents the zero-slope traveltime τ_0 mapped according to the oriented NMO formula in equation 15. These values predict correctly the reflection trajectories (red lines in Figure 4a) which then get warped until they are completely flattened (Figure 4c). Moreover, the oriented NMO does not introduce stretch effects as the traditional NMO processing. This is because the slope-based NMO applies a locally static shift to each data sample as opposed to to the dynamic one of the conventional NMO correction.

In conventional NMO processing, one scans a number of velocities, performs the corresponding moveout corrections, and picks the velocity trend from velocity spectra maxima. In the oriented processing, according to equations 16–18, anisotropy parameters become data attributes rather than prerequisites for imaging. Figure 5 shows the effective V_N, V_H and η values as data attributes mapped to the correct vertical time τ_0 position according to equation 15. These parameters have been obtained from the data through an automatic estimation of the local-slope field. The computational speed together with the automation are the main advantages of oriented processing.

Even though this synthetic data is noise-free, the slope and curvature estimates are not perfect. Nevertheless, Figure 5 shows a nearly constant trend along p direction of the recovered parameters that confirms the reliability of our method. Despite the large offset-to-depth ratio, we observe that V_H and η are more sensitive to the slope estimate uncertainty, which agrees with the observation of Tsvankin (2006) that high-order moveout parameters are in general less constrained than the short-spread

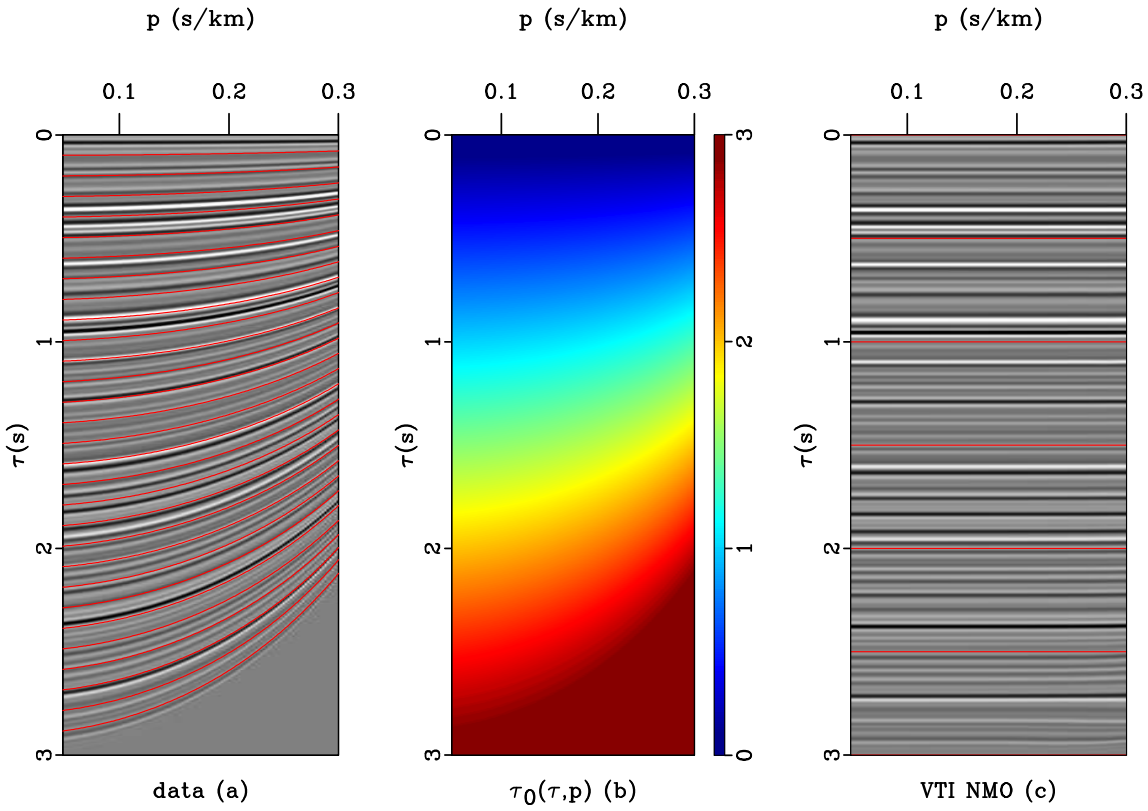

Figure 4: (b) Time mapping of each data sample from τ-p time to the zero-slope time τ_0 according to relation 15. These time values predict correctly reflection traveltime trajectory, the red lines in (a), which are then warped until they are completely flattened (c)

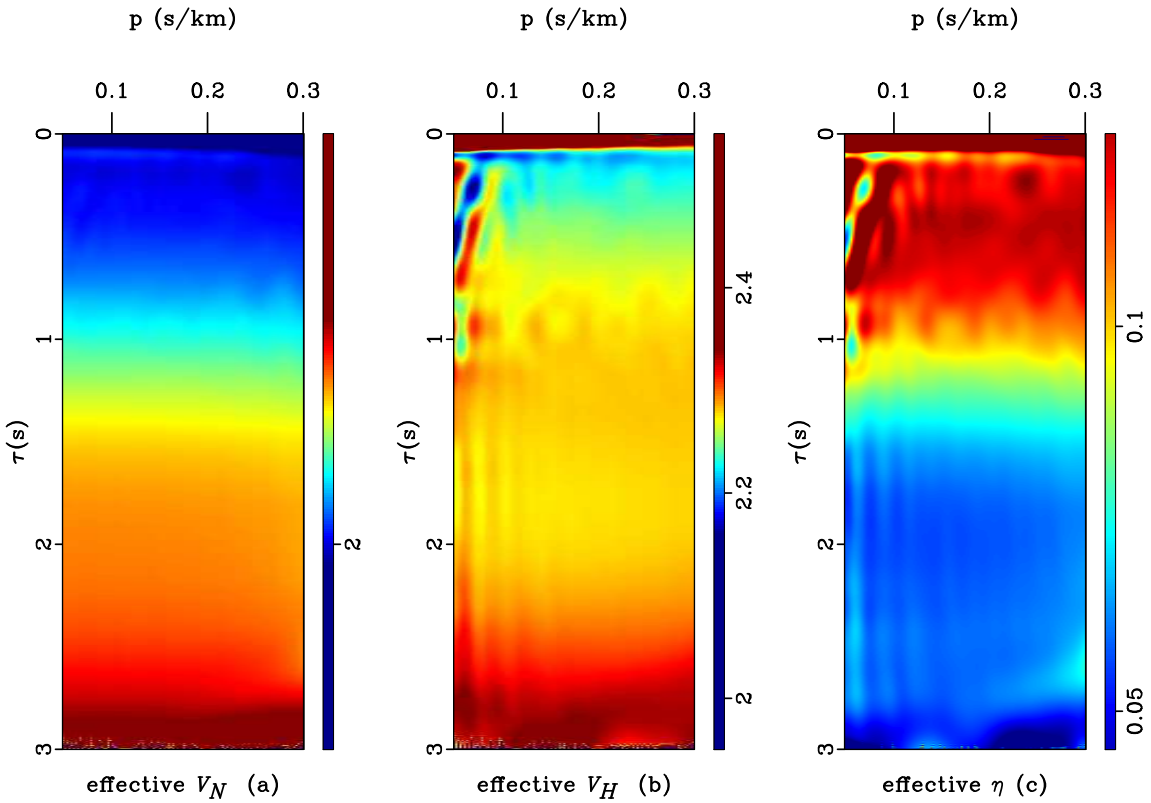

Figure 5: Effective normal moveout velocity (a), horizontal velocity (b) and anellipticity parameter η (c) computed as a data attribute through local estimate of slopes and curvature. These values are here mapped to the appropriate zero-slope τ_0 time using oriented NMO described by the equation 15.

normal moveout velocity V_N. The reduced data sensitivity to V_H and η at short offsets can explain the errors in the upper-right corner in panels (b) and (c) in Figure 5. A proper filtering procedure of the parameter maps may allow us to recover accurate parameter trends like those in Figure 6. The panels in Figure 6 represent semblance-like spectra computed by mapping each data sample to its parameter value at the zero-slope time τ_0. The yellow lines indicate the exact effective-parameter profiles used to generate the synthetic gather and confirm that our estimations follow the exact trends. Compared to conventional semblance spectra, these plots do not show the elongated "bull's eye" patterns which grow with increasing time. The improved resolution comes from the slope estimation accuracy and relates to the quality and complexity of the input data.

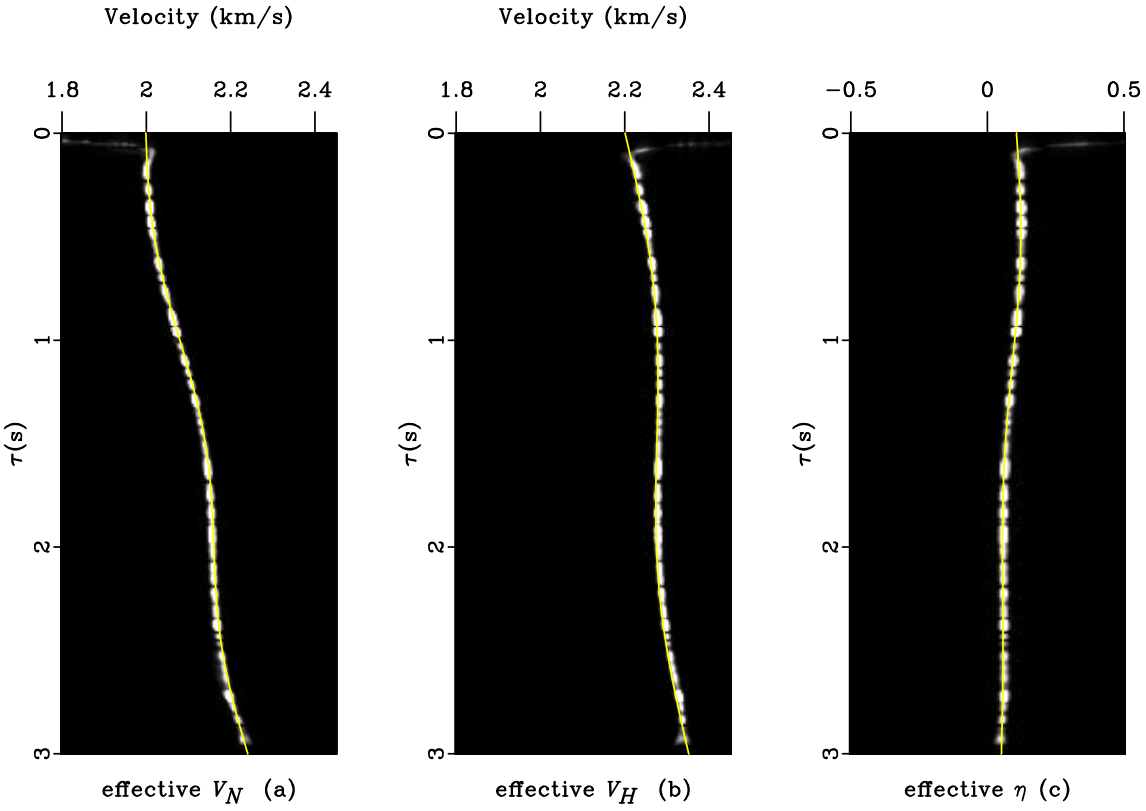

Figure 6: Effective normal moveout velocity (a), horizontal velocity (b) and anellipticity parameter η (c) semblance-like spectra. The yellow profiles indicate the exact effective values used for generating the synthetic data in Figure 3 (a). Compared to conventional semblance spectra, these plots do not show the elongated bull-eye pattern which enlarges with increasing time.

ESTIMATION OF INTERVAL PARAMETERS

Similarly to effective parameters, interval parameters can also be regarded as data attributes obtained from local slopes. Unlike the t-X domain, the τ-p domain offers us several alternatives to conventional Dix (1955) processing for retrieving interval values. In this section, we analyze three different options for extracting interval parameters in the τ-p domain.

		τ_0	R	Q	R_τ	Q_τ	$\tau_{0,\tau}$
Effective V_N V_H η		✓	✓	✓			
Interval $\hat{V}_N$ $\hat{V}_H$ $\hat{\eta}$	Dix	✓	✓	✓	✓	✓	
	Stripping	✓			✓	✓	
	Fowler	✓			✓		✓

Table 1: This table lists the inputs required to retrieve both effective and interval VTI parameters as data attributes obtained from local slopes. The zero-slope time τ_0 function is always required to map the attributes to their correct position in time. Processing data in τ-p domain offers two more alternatives than conventional Dix's processing in t-X domain. Moreover, we observe that Fowler's is the only set of equations that does not require an explicit use of the curvature.

Dix Inversion

Applying the chain rule, we rewrite the Dix inversion formula (Dix, 1955) as follows:

$$\hat{\mu} = \frac{d}{d\tau}\left[\tau_0(\tau)\mu(\tau)\right]\left[\frac{d\tau_0}{d\tau}\right]^{-1}. \tag{22}$$

where $\hat{\mu}$ is a vertically-variable interval parameter, μ is the corresponding effective parameter, and $\tau_0(\tau)$ is the zero-slope time mapping function. Substituting the LHS of equations 9 and 10 as μ and equation 15 as τ_0, we deduce expressions for the interval NMO velocity $\hat{V}_N$, horizontal velocity $\hat{V}_H$, and the anellipticity parameter $\hat{\eta}$. The derivations and the final formulas are detailed in appendix B. In order to retrieve interval parameters by slope-based Dix inversion, one needs as inputs the slope R and the curvature Q fields as well as their derivatives along the time axis τ (see Table 1). This confirms that, even in τ-p , an application of Dix's formula requires the knowledge of the effective quantities which, in this context, are mathematically represented by the slope R and curvature Q. The τ_0 mapping field is also needed to map the estimated VTI parameters to the correct imaging time. The Dix inversion route does not seem very practical in the τ-p domain because the equations (derived in appendix B) appear cumbersome.

Claerbout's straightedge method

Claerbout (1978) suggested that interval velocity in an isotropic ($\hat{V}_N = \hat{V}_H$) layered medium could be estimated with a *pen and a straightedge* by measuring the offset difference Δx between equal slope p points on two reflection events (Figure 1a). The computation of Δx is straightforward after a CMP gather has been transformed into the τ-p domain. In fact, the τ-p transform naturally aligns seismic events with equal slope along the same trace (Figure 1b). Moreover, local slopes $R(\tau, p) = d\tau/dp$ are related to the emerging offset $x = -R$ (van der Baan, 2004) , therefore Claerbout's inversion formula can be expressed as

$$\hat{V}_N^2(\tau, p) = \frac{R_\tau}{p^2 R_\tau - p}, \tag{23}$$

where $R_\tau = \partial R(\tau, p)/\partial \tau$ and $\hat{V}_N$ is the NMO interval velocity that we map back to zero-slope time τ_0 using the isotropic velocity independent τ-p NMO, as suggested by Fomel (2007b). The details of the derivation are in appendix C.

The two methods discussed next can be thought of as two alternative extensions for VTI media of the original Claerbout's straightedge method.

Stripping equations

The first alternative to the Dix inversion is what we call *stripping equations* (Casasanta and Fomel, 2010). Starting from the integral equation 7 for τ-p reflection moveout and employing the chain rule (equation C-4), we first deduce an expression for slope R_τ (equation C-5) and curvature Q_τ (equation C-6) using τ-derivatives, that now depend on the interval parameters. Then, solving for $\hat{V}_N$ and $\hat{V}_H$, we obtain the following expressions:

$$\hat{V}_N^2(\tau, p) = -\frac{1}{p}\frac{16 R_\tau^3}{\hat{N}\hat{D}}, \tag{24}$$

$$\hat{V}_H^2(\tau, p) = \frac{1}{p^2}\frac{\hat{N} - 4R_\tau}{\hat{N}}, \tag{25}$$

and

$$\hat{\eta}(\tau, p) = \frac{1}{p}\frac{\hat{N}(4R_\tau - \hat{D})}{32\tau R_\tau^3}, \tag{26}$$

which provide an estimate for the interval parameters. In the above equations, $\hat{N} = pQ_\tau + 3R_\tau - 3pR_\tau^2$ and $\hat{D} = pQ_\tau + 3R_\tau + pR_\tau^2$, which corresponds to the interval values of the numerator N and denominator D of the square root in equation 15. These relations are very similar to those previously derived for the effective parameters (equations 16–18). However, they require the τ derivative of the slope and curvature fields (Table 1). This result agrees with the discussion above about layer stripping in τ-p. In this domain, layer stripping reduces to computing traveltime differences

(equation 4) at each horizontal slowness p. Therefore, differentiating the effective slope R and curvature Q fields in τ provides the necessary information to access the interval parameters directly. This is the power of the τ-p domain as opposed to t-X , where the only practical path to interval parameters is through Dix inversion that requires the knowledge of effective parameters. The zero-slope time τ_0 is needed to map the interval parameter estimates to the correct vertical time (Table 1).

Fowler's equations

The second alternative to get VTI interval parameters comes from the integral formulation of the τ-p moveout signature in equation 7. The derivation is detailed in Appendix C. We first compute $\tau_{0,\tau} = \partial\tau_0/\partial\tau$ and then, applying the chain rule, R_τ. Solving for $\hat{V}_N$ and $\hat{V}_H$, we arrive at the following relations:

$$\hat{V}_N^2(\tau, p) = -\frac{[\tau_{0,\tau}^2 - 1]^2}{p^3 \tau_{0,\tau}^2 \, R_\tau}, \tag{27}$$

$$\hat{V}_H^2(\tau, p) = \frac{\tau_{0,\tau}^2[1 - R_\tau] + 1}{p^3 \tau_{0,\tau}^2 \, R_\tau}, \tag{28}$$

which are equivalent to those proposed previously by Fowler et al. (2008). According to equations 27 and 28, the gradients of offset x and the zero-slope time τ_0 measured at common slope locations p on two consecutive seismic event return the VTI interval parameters for the layer bounded by these two events (Figure 1a). Fowler et al. (2008) first pick traveltime curves in t-X domain, and then differentiate those curves in offset to compute slopes p. Finally, for any given p value on each seismic event, they determine the corresponding Δx and $\Delta\tau_0$ values (Figure 1a). The main practical limitation in this inversion scheme is the difficulty of picking seismic events accurately.

The processing becomes easier if it is accomplished in τ-p with automatic slope estimation. First, τ-p transform unveils the position of equal slope events. Second, $\tau_{0,\tau}$ and R_τ are measured automatically (without event picking) on the τ-p transformed CMP gather. The quantity $\tau_{0,\tau}$ can be estimated as the τ finite difference of τ_0 values computed according to velocity-independent moveout equation 15. The zero-slope time τ_0 function is still needed to map the interval parameter estimated using equations 27 and 28 to the correct vertical time (Table 1).

FLATTENING BY PREDICTIVE PAINTING

As shown in Table 1, Fowler's is the only set of equations that do not require an explicit use of the curvature Q. The dependence on the curvature is absorbed by the τ_0 function. The other two sets of equations, Dix and stripping formulas, as well as the equations for effective parameters, do need curvature. The curvature computation can be problematic when the data are contaminated by noise. This makes these three

methods (effective, stripping, and Dix) less practical when applied to real data with poor SNR. However, Fowler's rules represent a way to circumvent the problem. In fact, if we can find an algorithm that estimates the τ_0 mapping function directly from the data, all the curvature issues will get solved.

The desired algorithm exists and is known as seismic image flattening. The idea of using local slopes for automatic flattening was introduced by Bienati and Spagnolini (2001) and Lomask et al. (2006). Flattening by predictive painting (appendix A) uses the local-slope field to construct a recursive prediction operator (equation A-4) that spreads a traveltime reference trace in the image and predicts the reflecting surfaces which are then unwrapped until the image is flattened.

We propose bypassing the issue of estimating the zero-slope time τ_0 field by using the predictive painting approach. Let us discuss how it works on the previously shown synthetic data in Figure 7a. Figure 7b shows local event slope R measured from the data using the PWD algorithm. Figure 7c shows how predictive painting spreads a zero-slope time τ_0 reference trace along local data slopes to predict the zero-slope time τ_0 mapping field and hence the geometry of the traveltime reflection curves along τ-p CMP gather. Because this procedure does not involve curvature computations, it represents a much more robust way of obtaining the τ_0 field that is needed by the inversion formulas in equations 27 and 28. After τ_0 has been found, we also have what we need to perform gather flattening (Burnett and Fomel, 2009a,b). Unshifting each trace (Figure 7d) automatically flattens the data, thus performing a velocity-independent τ-p NMO correction. As expected, all events are perfectly aligned, and the correction does not suffer from instabilities of curvature estimation. Moreover, predictive painting is automatic and does not require any prior assumptions about the moveout shape.

Now, given the slope field R and its zero-slope time field τ_0, we retrieve interval parameters using equations 27 and 28. In Figure 8, the estimated NMO (a) horizontal velocities (b) and the anellipticity (c) parameter are mapped to the appropriate zero-slope time using the painted zero-slope time τ_0 field (Figure 7c). The exact interval profiles (yellow lines) are recovered nearly perfectly although the resolution slightly worsens with respect to the effective profiles (Figure 6). The main reason is the instability of the additional numerical differentiation along the τ direction that all the approaches require.

FIELD DATA EXAMPLE

Figure 9 presents the results of the proposed τ-p processing on a field data example from a marine acquisition. Figure 9a shows a τ-p transformed CMP gather. The data are taken from a deep water (3.5 s of sea-depth) dataset with poor offset sampling ($\sim 100\ m$) that aliases the steepest seismic events. Spatial aliasing creates artifacts in τ-p domain that bias the PWD slope estimate. In order to mitigate the effect of the aliasing, we interpolated the raw data by means of an FX algorithm (Spitz, 1991).

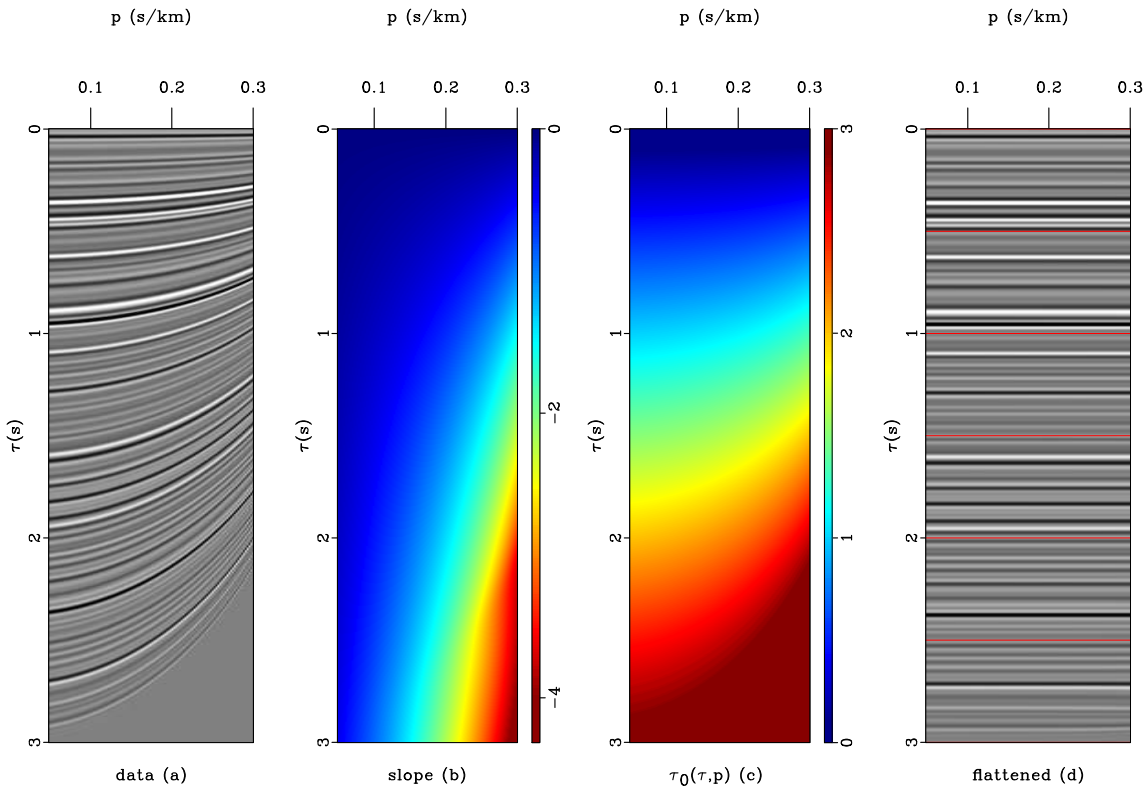

Figure 7: Synthetic CMP τ-p transformed gather (a), estimated local slopes (b), zero slope time τ_0 obtained by predictive painting (c), and the gather flattened (d).

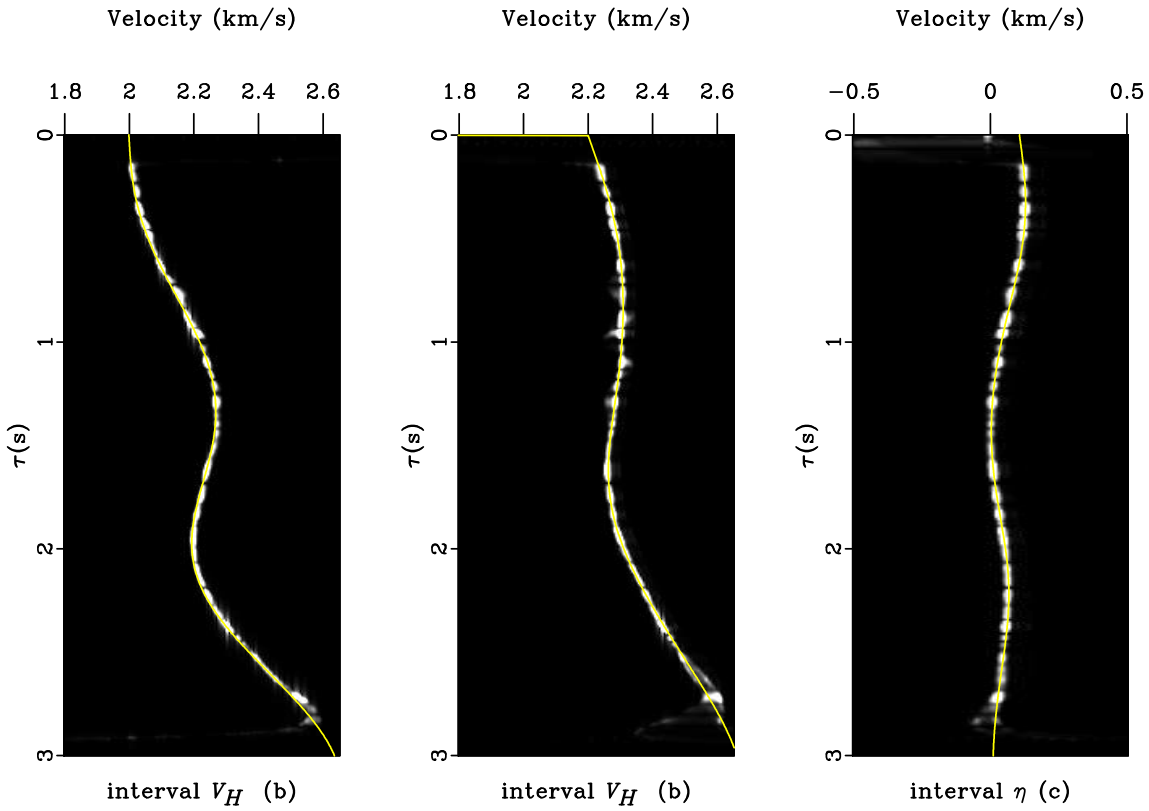

Figure 8: Fowler's equation based inversion to interval normal moveout (a) horizontal velocity (b) and anellipticity parameter η (c). The yellow lines represent the exact values used for generating the synthetic dataset in figure 3 (a).

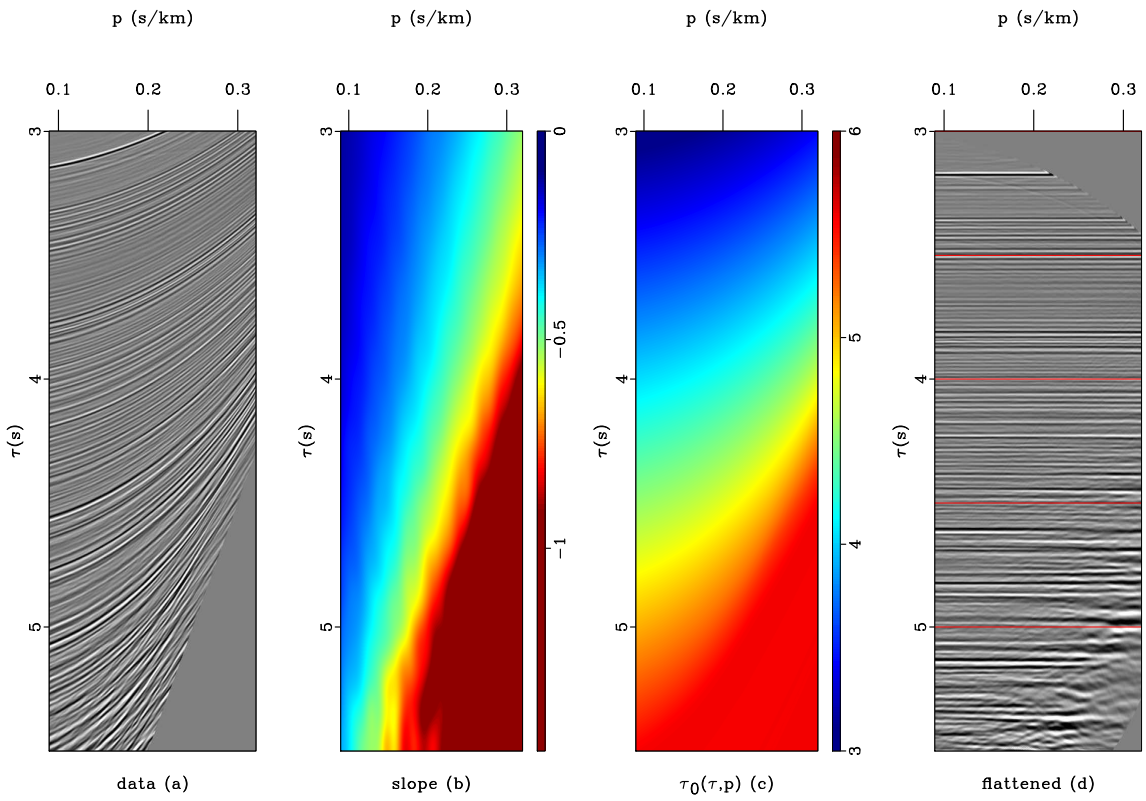

Figure 9: τ-p or Radon transformed data from a marine acquisition (a). The data are fairly clean even though there is a slight decrease in SNR for later and steepest events. The CMP maximum offset-to-depth ratio reaches 1.5 for larger value of the horizontal slope p. Dominant local-slope field (b) measured using PWD algorithm. Using the slopes we estimate the zero-slope time τ_0 mapping fields (c) that predicts reflection curves by which we flatten the original gather (d).

The original trace recording is 7.0 s long but, since the SNR decreases significantly after 5.0 s, we window the CMP gather and process seismic events only between 3.0 and 6.0 s. The CMP maximum offset-to-depth ratio reaches 1.5 for larger value of the horizontal slope p. As for the synthetic case, the data should carry enough information to well resolve the horizontal velocity and the anellipticity parameter. Figure 9b shows the dominant local-slope R field automatically measure from the data using the PWD algorithm. As in the synthetic case, we use these slopes to construct the prediction operator that allows us to paint the zero-slope traveltime map τ_0 along the reflection events (Figure 9c). The τ_0 values are finally used to unwrap the trace shifts until the gather is completely flattened. The good alignment of the NMO corrected traces (Figure 9d) confirms the robustness of predictive painting with real data. Figure 10 shows spectra of the recovered interval parameters using Fowler's equations 27 and 28. The plots are overlaid with the profiles (yellow curves) recovered using a layer-based t-X Dix inversion (Ferla and Cibin, 2009) and by the profiles obtained after an automated picking of the recovered trends. Our solution (red curves) follows the Dix trends (yellow curves) even though it exhibits a slight decrease in accuracy. The poor SNR for later and steeper events and the numerical differentiation of the zero-slope traveltime τ_0 and slope R make the field data results noisier. As expected, the high-order moveout parameters appear to be more sensitive to the noise. Moreover, the more pronounced enlargement of the $\hat{\eta}$ trend in comparison with the $\hat{V}_H$ trend confirms that the latter parameter is better constrained by the data (Tsvankin, 2006).

DISCUSSION

In the conventional NMO processing, one needs to scan over a range of possible velocities and pick the appropriate velocity trend from semblance maxima. Therefore, the cost of velocity scanning is roughly proportional to the number of scanned velocities N_V times the input data size. Anisotropic velocity analysis is performed by simultaneously scanning two (or more) parameters. Consequently, the number of trial velocities/parameters squares, which increases the computational time dramatically. In oriented processing, the effective anisotropy parameters turn into data attributes according to equations 16–18. These parameters are directly mapped from the slope field R to the correct zero-slope/offset traveltime τ_0. The cost of local slope estimation with plane-wave destruction method is proportional to the data size times the number of estimation iterations N_I times the 2D filter size N_F. Typically $N_I = 10$ and $N_F = 6$, which roughly correspond to scanning $N_V = 60$ velocities. However, unlike semblance analysis, this cost does not increase if we are estimating one, two or more parameters. The cost of the semblance scan becomes even more prohibitive when processing wide-azimuth data. The computational advantages of our approach are encouraging especially with respect to multi-azimuth processing and orthorhombic velocity analysis, where time processing is controlled by at least five parameters (Tsvankin, 2006).

Automation, in addition to speed, is another clear advantage of the slope-based

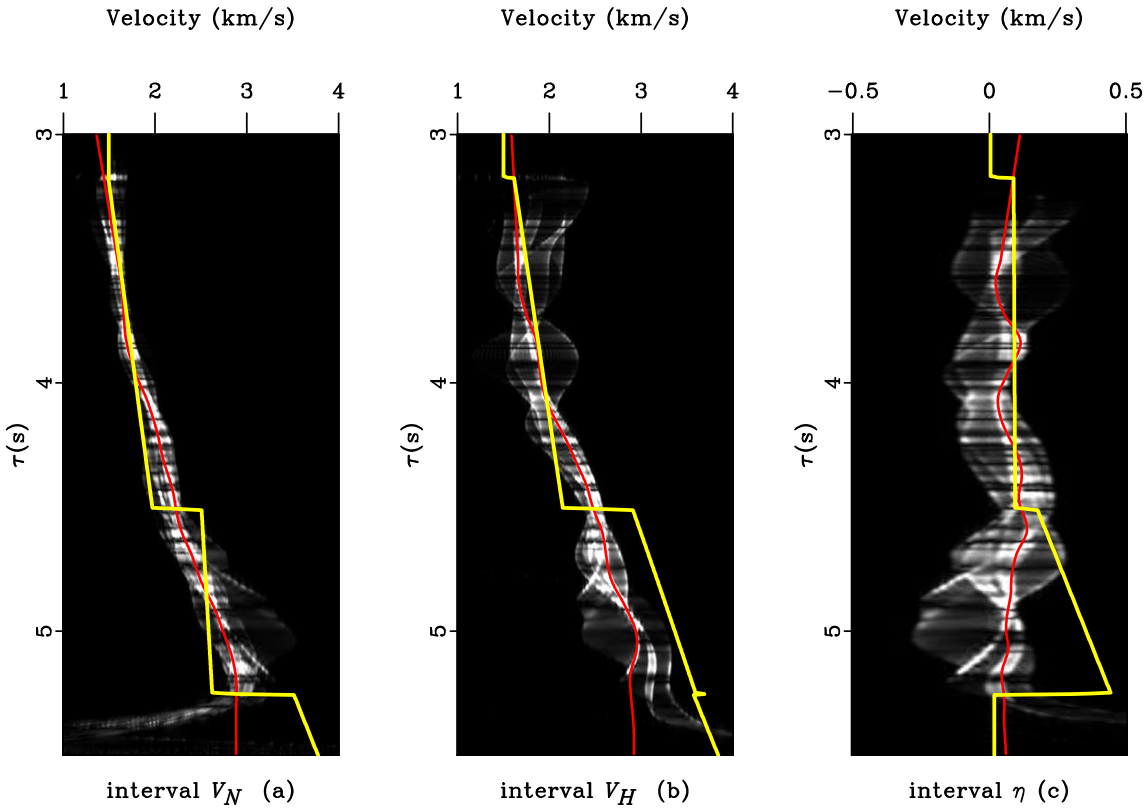

Figure 10: Parameters spectra for interval normal moveout (a), horizontal velocity (b) and anellipticity parameter η (c). These spectra result from the application of Fowler's equations using painted τ_0 field. The red lines are the profiles after an automated picking of the estimated spectra. The yellow lines are the recovered profiles after a layer-based t-X Dix inversion procedure (Ferla and Cibin, 2009).

processing. Slope estimation provided by plane-wave destruction represents an automated approach to velocity analysis. It may require a limited user-interaction in choosing input parameters. A user-supplied initial guess for the slope field can accelerate the nonlinear optimization , thereby providing a more reliable estimate for the slopes. The smoothness of the output slopes is controlled by shaping regularization; the length of a 2-D triangular smoothing filter controls smoothness along p and τ direction in the τ-p transformed CMP data. If the input seismic data are not regularly and properly sampled in space, as often happens in wide-azimuth acquisition, the τ-p transform may add to the data coherent-noise artifacts. This can affect the final result of PWD slope estimation. Thus, if the seismic τ-p data are noisy, increasing the length of smoothing filters can help in achieving a more stable solution, despite some loss in resolution. In contrast, for high SNR data, less smoothing yields better-resolved slope fields.

All the equations we have developed in this paper hold for S-wave data as long as we use two parameters S-wave phase-velocity approximation (Stovas, 2009). The combination of the results from P-wave and S-wave processing may enable a retrieval of all the elastic parameters needed to build an initial VTI anisotropic model suitable for depth processing.

The application of the proposed method is also limited by the underlying assumption of vertical variation of the velocity model with the horizontal symmetry plane. In principle, the method can handle limited lateral variation of the velocity. Therefore, it can be used for dense anisotropic moveout analysis at the early stages of processing.

CONCLUSIONS

Local slopes of seismic events carry complete information about the structure of the subsurface. We have developed a velocity-independent τ-p imaging approach to perform moveout correction in 2D layered VTI media. We process Radon-transformed data because τ-p is the natural domain for anisotropic parameter estimation in vertically-variable media. Effective VTI parameters turn into data attributes through the use of slopes and are directly mappable to the zero-slope traveltime. Interval parameters turn into data attributes as well. We have developed the analytical theory for the slope-based Dix inversion in τ-p , as well as two alternative sets of equations that can be regarded as an extension of Claerbout's method for *straightedge determination of interval velocity*. Both sets of equations exploit the intrinsic layer stripping power of the τ-p domain to estimate interval parameters directly without involving effective parameters.

The equations we have introduced to retrieve both effective and interval parameters in VTI media require directly or indirectly an estimation of the local data curvature. On the other hand, Fowler's equations do not require an explicit use of the curvature. Therefore, we propose bypassing the curvature estimation by exploiting a curvature-independent estimation of the zero-slope time τ_0 field that, together

with the slopes, provides the input to Fowler's method. The zero-slope time can be found efficiently by employing the predictive painting algorithm. A reference trace at the zero-slope time τ_0 is spread along the local data slope to predict the τ_0 field along reflection curves in the τ-p CMP gather. This estimation appears robust and efficient enough to enable automated, slope-based, dense estimation of interval parameters.

ACKNOWLEDGMENTS

The first author thanks Nicola Bienati, Paul Fowler, and Ilya Tsvankin for fruitful and stimulating discussions. A special acknowledgment goes to Giuseppe Drufuca and the members of the DSP(GEO) research group at Politecnico di Milano for their support. The second author acknowledges partial financial support from ExxonMobil and RPSEA[1] and thanks Tariq Alkhalifah, Will Burnett, and Yang Liu for helpful discussions. Both the authors are indebted to Alexey Stovas and the anonymous reviewer for their excellent reviews. Their suggestions and insightful remarks have improved the clarity of the paper.

REFERENCES

Al-Dajani, A., and I. Tsvankin, 1998, Nonhyperbolic reflection moveout for horizontal transverse isotropy: Geophysics, **63**, 1738–1753.

Alkhalifah, T., 1997, Velocity analysis using nonhyperbolic moveout in transversely isotropic media: Geophysics, **62**, 1839–1854.

———, 1998, Acoustic approximations for processing in transversely isotropic media: Geophysics, **63**, 623–631.

———, 2000, An acoustic wave equation for anisotropic media: Geophysics, **65**, 1239–1250.

Alkhalifah, T., and I. Tsvankin, 1995, Velocity analysis for transversely isotropic media: Geophysics, **60**, 1550–1566.

Bienati, N., and U. Spagnolini, 2001, Multidimensional wavefront estimation from differential delays: IEEE Trans. on Geoscience and Remote Sensing, **39**, 655–664.

Burnett, W., and S. Fomel, 2009a, 3D velocity-independent elliptically anisotropic moveout correction: Geophysics, **74**, WB129–WB136.

———, 2009b, Moveout analysis by time-warping: SEG Technical Program Expanded Abstracts, **28**, 3710–3714.

[1]The funding by RPSEA was provided through the *Ultra-Deepwater and Unconventional Natural Gas and Other Petroleum Resource* program authorized by the U.S. Energy Policy Act of 2005. RPSEA (`www.rpsea.org`) is a nonprofit corporation whose mission is to provide a stewardship role in ensuring the focused research, development and deployment of safe and environmentally responsible technology that can effectively deliver hydrocarbons from domestic resources to the citizens of the United States. RPSEA, operating as a consortium of premier U.S. energy research universities, industry, and independent research organizations, manages the program under a contract with the U.S. Department of Energy's National Energy Technology Laboratory.

Byun, B. S., D. Corrigan, and J. E. Gaiser, 1989, Anisotropic velocity analysis for lithology discrimination: Geophysics, **54**, 1564–1574.

Casasanta, L., and S. Fomel, 2010, Velocity independent τ-p moveout in layered VTI media: 72nd EAGE Conference & Exhibition, EAGE, Expanded Abstract C030.

Claerbout, J., 1992, Earth sounding analysis: Processing versus inversion: Blackwell.

Claerbout, J. F., 1978, Straightedge determination of interval velocity, *in* SEP-14: Stanford Exploration Project, 13–16.

de Bazelaire, E., 1988, Normal moveout revisited: Inhomogeneous media and curved interfaces: Geophysics, **53**, 143–157.

Dix, C. H., 1955, Seismic velocities from surface measurements: Geophysics, **20**, 68–86.

Douma, H., and M. van der Baan, 2008, Rational interpolation of qP-traveltimes for semblance-based anisotropy estimation in layered VTI media: Geophysics, **73**, D53–D62.

Ferla, M., and P. Cibin, 2009, Interval anisotropic parameters estimation in a least squares sense — application on congo mtpn real dataset: SEG Technical Program Expanded Abstracts, **28**, 296–300.

Fomel, S., 2002, Applications of plane-wave desctruction filters: Geophysics, **67**, 1946–1960.

———, 2004, On anelliptic approximations for qP velocities in VTI media: Geophysical Prospecting, **52**, 247–259.

———, 2007a, Shaping regularization in geophysical estimation problems: Geophysics, **72**, R29–R36.

———, 2007b, Velocity-independent time-domain seismic imaging using local event slopes: Geophysics, **72**, S139–S147.

———, 2008, Nonlinear shaping regularization in geophysical inverse problems: SEG Technical Program Expanded Abstracts, **27**, 2046–2051.

———, 2010, Predictive painting of 3d seismic volumes: Geophysics, **75**, A25–A30.

Fomel, S., and A. Stovas, 2010, Generalized nonhyperbolic moveout approximation: Geophysics, **75**, U9–U18.

Fowler, P. J., A. Jackson, J. Gaffney, and D. Boreham, 2008, Direct nonlinear traveltime inversion in layered VTI media: SEG Technical Program Expanded Abstracts, **27**, 3028–3032.

Lambaré, G., 2008, Stereotomography: Geophysics, **73**, VE25–VE34.

Lambaré, G., M. Alerini, R. Baina, and P. Podvin, 2003, Stereotomography : A fast approach for velocity macro-model estimation: SEG Technical Program Expanded Abstracts, **22**, 2076–2079.

Lomask, J., A. Guitton, S. Fomel, J. Claerbout, and A. A. Valenciano, 2006, Flattening without picking: Geophysics, **71**, P13–P20.

Ottolini, R., 1983, Velocity independent seismic imaging: Technical report, Stanfor Exploration Project.

Riabinkin, L. A., 1957, Fundamentals of resolving power of controlled directional reception (CDR) of seismic waves, *in* Slant-stack processing, 1991: Soc. of Expl. Geophys. (Translated and paraphrased from *Prikladnaya Geofiizika*, **16**, 3-36), 36–60.

Rieber, F., 1936, A new reflection system with controlled directional sensitivity: Geophysics, **1**, 97–106.

Roganov, Y., and A. Stovas, 2011, Caustics in a periodically layered transversely isotropic medium with vertical symmetry axis: Geophysical Prospecting, DOI: 10.1111/j.1365–2478.2010.00924.x.

Sil, S., and M. Sen, 2008, Azimuthal τ-p analysis in anisotropic media: Geophysical Journal International, **175**, 587–597.

Siliqi, R., and N. Bousquié, 2000, Anelliptic time processing based on a shifted hyperbola approach: SEG Technical Program Expanded Abstracts, **19**, 2245–2248.

Siliqi, R., P. Herrmann, A. Prescott, and L. Capar, 2007, High-order RMO picking using uncorrelated parameters: SEG Technical Program Expanded Abstracts, **26**, 2772–2776.

Spitz, S., 1991, Seismic trace interpolation in the F-X domain: Geophysics, **56**, 785–794.

Stovas, A., 2009, Direct Dix-type inversion in a layered VTI medium: SEG Technical Program Expanded Abstracts, **28**, 2506–2510.

Stovas, A., and S. Fomel, 2010, The generalized non-elliptic moveout approximation in the τ-p domain: SEG Technical Program Expanded Abstracts, 253–257.

Sword, C. H., 1987, Tomographic determination of interval velocities from reflection seismic data: The method of controlled directional reception: PhD thesis, Stanford University.

Taner, M. T., and F. Koehler, 1969, Velocity spectra—digital computer derivation applications of velocity functions: Geophysics, **34**, 859–881.

Thomsen, L., 1986, Weak elastic anisotropy: Geophysics, **51**, 1954–1966.

Tsvankin, I., 1995, Normal moveout from dipping reflectors in anisotropic media: Geophysics, **60**, 268–284.

———, 2006, Seismic signatures and analysis of reflection data in anisotropic media: Elsevier.

Tsvankin, I., J. Gaiser, V. Grechka, M. van der Baan, and L. Thomsen, 2010, Seismic anisotropy in exploration and reservoir characterization: An overview: Geophysics, **75**, 75A15–75A29.

Ursin, B., and A. Stovas, 2006, Traveltime approximations for a layered transversely isotropic medium: Geophysics, **71**, D23–D33.

van der Baan, M., 2004, Processing of anisotropic data in the tau-p domain: I—Geometric spreading and moveout corrections: Geophysics, **69**, 719–730.

van der Baan, M., and J. M. Kendall, 2002, Estimating anisotropy parameters and traveltimes in the tau-p domain: Geophysics, **67**, 1076–1086.

Wang, X., and I. Tsvankin, 2009, Estimation of interval anisotropy parameters using velocity-independent layer stripping: Geophysics, **74**, WB117–WB127.

Wolf, K., D. Rosales, A. Guitton, and J. Claerbout, 2004, Robust moveout without velocity picking: SEG Technical Program Expanded Abstracts, **23**, 2423–2426.

Yilmaz, O., 2000, Seismic data analysis: SEG.

APPENDIX A

LOCAL PLANE-WAVES OPERATORS

Local plane-wave operators model seismic data (Fomel, 2002) . The mathematical basis is the local plane differential equation

$$\frac{\partial P}{\partial x} + \sigma \frac{\partial P}{\partial t} = 0 \; , \tag{A-1}$$

where $P(t,x)$ is the wave field and σ the local slope field (Claerbout, 1992). In the case of a constant slope, the solution of equation A-1 is a simple plane wave $P(t,x) = f(t - \sigma x)$ where $f(t)$ is an arbitrary waveform. Assuming that the slope $\sigma = \sigma(t,x)$ varies in time and space, one can design a local operator to propagate each trace to its neighbors. Let $\mathbf{s}$ represent a seismic section as a collection of traces: $\mathbf{s} = [\mathbf{s}_1 \; \mathbf{s}_2 \; \dots \; \mathbf{s}_N]^T$, where $\mathbf{s}_k$ corresponds to $P(t,x_k)$ for $k = 1, 2, \dots$ A plane-wave destruction operator (PWD) effectively predicts each trace from its neighbor and subtracts the prediction from the original trace (Fomel, 2002). In linear operator notation, the plane-wave destruction operation can be defined as

$$\mathbf{r} = \mathbf{D}(\sigma)\, \mathbf{s} \; , \tag{A-2}$$

where $\mathbf{r}$ is the destruction residual, and $\mathbf{D}$ is the destruction operator defined as

$$\mathbf{D}(\sigma) = \begin{bmatrix} \mathbf{I} & 0 & 0 & \cdots & 0 \\ -\mathbf{P}_{1,2}(\sigma) & \mathbf{I} & 0 & \cdots & 0 \\ 0 & -\mathbf{P}_{2,3}(\sigma) & \mathbf{I} & \cdots & 0 \\ \cdots & \cdots & \cdots & \cdots & \cdots \\ 0 & 0 & \cdots & -\mathbf{P}_{N-1,N}(\sigma) & \mathbf{I} \end{bmatrix} \; , \tag{A-3}$$

where $\mathbf{I}$ stands for the identity operator, and $\mathbf{P}_{i,j}(\sigma)$ describes prediction of trace j from trace i. Prediction of a trace consists of shifting the original trace along dominant event slopes σ. The dominant slopes are estimated by minimizing the prediction residual $\mathbf{r}$ in a least-squares sense. Since the prediction operators A-3 depends on the slopes themselves, the inverse problem is nonlinear and must be solved in a iterative fashion by subsequent linearizations. We employ shaping regularization (Fomel, 2007a) for controlling the smoothness of the estimated slope field.

Once the local slope field σ has been computed, prediction of a trace from a distant neighbor can be accomplished by simple recursion. Predicting trace k from trace 1 is

$$\mathbf{P}_{1,k} = \mathbf{P}_{k-1,k} \cdots \mathbf{P}_{2,3}\, \mathbf{P}_{1,2} \; . \tag{A-4}$$

If $\mathbf{s}_r$ is a reference trace, then the prediction of trace $\mathbf{s}_k$ is $\mathbf{P}_{r,k}\, \mathbf{s}_r$. Fomel (2010) called the recursive operator $\mathbf{P}_{r,k}$ predictive painting. The elementary prediction operators in equation A-3 spread information from a given trace to its neighbors recursively by following the local structure of seismic events. Figure 7 in the main text illustrates the painting concept.

APPENDIX B

MATHEMATICAL DERIVATION OF SLOPE-BASED DIX INVERSION

The Dix formula (Dix, 1955) can be written in the differential form

$$\hat{\mu} = \frac{d}{d\tau_0}\left[\tau_0 \mu(\tau_0)\right], \tag{B-1}$$

where $\hat{\mu}$ is the interval parameter corresponding to zero-slope time τ_0 and $\mu(\tau_0)$ is the vertically-variable general effective parameter. Using the chain rule, we rewrite the Dix's formula B-1 as follows:

$$\hat{\mu} = \frac{d}{d\tau}\left[\tau_0(\tau)\mu(\tau)\right]\left[\frac{d\tau_0}{d\tau}\right]^{-1}. \tag{B-2}$$

At first, let us consider the VTI NMO velocity as an effective parameter, hence $\mu = V_N^2$. Using the expression for $\tau_0(\tau)$ (equation 15) and $V_N^2(\tau)$ (equation 16), we obtain, after some algebra,

$$\frac{d\tau_0}{d\tau} = \frac{1}{2\tau_0}\frac{\tau(2ND + \tau(N_\tau D - D_\tau N))}{D^2}, \tag{B-3}$$

$$\frac{d\left[\tau_0(\tau)V_N^2(\tau)\right]}{d\tau} = -\frac{8\tau^2 R^2(\tau)\left[6\tau DNR_\tau - \tau DRN_\tau - 3\tau NRD_\tau + 4DNR\right]}{pD^3 N\tau_0}, \tag{B-4}$$

where $R_\tau = \partial R/\partial\tau$, $Q_\tau = \partial Q/\partial\tau$ and

$$N_\tau = \partial N/\partial\tau = (3\tau - 6pR)\,R_\tau + p\tau Q_\tau + 3R + pQ, \tag{B-5}$$

$$D_\tau = \partial D/\partial\tau = (3\tau + 2pR)\,R_\tau + p\tau Q_\tau + 3R + pQ. \tag{B-6}$$

Inserting equation B-3 and B-4 in B-2 leads to

$$\hat{V}_N = -\frac{16\tau R^2}{pDN}\frac{\left[6\tau DNR_\tau - \tau DRN_\tau - 3\tau NRD_\tau + 4DNR\right]}{\left[2ND + \tau N_\tau D - \tau D_\tau N\right]} \tag{B-7}$$

.

To compute the interval $\hat{V}_H$ or $\hat{\eta}$, we employ as effective value $\mu = S\ V_N^4$ as described in equation 10. In this case, the modified Dix formula (equation B-2) can be rewritten as follows

$$\hat{S} = \frac{1}{\hat{V}_N^4(\tau)}\frac{d}{d\tau}\left[\tau_0(\tau)S(\tau)V_N^4(\tau)\right]\left[\frac{d\tau_0}{d\tau}\right]^{-1}, \tag{B-8}$$

which, after substituting the chain relation for the interval $\hat{V}_N^2(\tau) = \frac{d\left[\tau_0(\tau)V_N^2(\tau)\right]}{d\tau}\left[\frac{d\tau_0}{d\tau}\right]^{-1}$ and some simplifications, leads to the relation

$$\hat{S} = S(\tau)\frac{V_N^2(\tau)}{\hat{V}_N^2(\tau)} + \tau_0(\tau)\frac{V_N^2(\tau)}{\hat{V}_N^4(\tau)}\frac{d}{d\tau}\left[S(\tau)V_N^2(\tau)\right]\left[\frac{d\tau_0}{d\tau}\right]^{-1}, \tag{B-9}$$

which involves only the mapping relations for the zero-slope time $\tau_0(\tau)$ (formula 15) effective NMO velocity $V_N^2(\tau)$ (formula 16), and the anellipticity parameter obtained by equation 18 as $S(\tau) = 1 + 8\eta(\tau)$. From the interval parameter $\hat{S}$, we can go back to interval $\hat{V}_H^2 = \hat{V}_N^2\,(\hat{S}+3)/4$ and $\hat{\eta} = (\hat{S}-1)/8$.

In the case of isotropy or elliptical anisotropy ($\hat{V}_N = \hat{V}_H$), equations B-3 and B-4 simplify to

$$\frac{d\tau_0}{d\tau} = \frac{2\tau - p(R + \tau R_\tau)}{2\tau_0}, \tag{B-10}$$

$$\frac{d\left[\tau_0(\tau)V_N^2(\tau)\right]}{d\tau} = \frac{1}{2}\frac{pR(R+\tau R_\tau) - 2R_\tau\tau^2}{\tau_0 p(pR-\tau)} \tag{B-11}$$

Inserting equations B-10 and B-11 in formula B-2, we get

$$\hat{V}_N = \frac{1}{p(pR-\tau)}\frac{pR(R+\tau R_\tau) - 2R_\tau\tau^2}{2\tau - p(R+\tau R_\tau)}. \tag{B-12}$$

This equation is the analog of equation 15 in (Fomel, 2008).

APPENDIX C

MATHEMATICAL DERIVATION OF STRIPPING EQUATIONS

Starting from the integral representation of τ-p signature in equation 7, we arrive at the expression of the slope R and the curvature Q fields as the following integrals:

$$R(\tau_0, p) = \int_0^{\tau_0} \mathcal{F}'(p,\xi)d\xi, \tag{C-1}$$

$$Q(\tau_0, p) = \int_0^{\tau_0} \mathcal{F}''(p,\xi)d\xi, \tag{C-2}$$

where

$$\mathcal{F}(\tau_0, p) = \sqrt{\frac{1 - \hat{V}_H^2(\tau_0)p^2}{1 - [\hat{V}_H^2(\tau_0) - \hat{V}_N^2(\tau_0)]p^2}}\,,$$

$\mathcal{F}' = \frac{d\mathcal{F}}{dp}$ and $\mathcal{F}'' = \frac{d^2\mathcal{F}}{dp^2}$. According to equation 7, it descends that

$$\tau_{0,\tau}(\tau, p) = \left[\frac{\partial\tau_0}{\partial\tau}\right]^{-1} = \frac{1}{\mathcal{F}(p,\tau)}. \tag{C-3}$$

Therefore, applying the chain rule

$$\frac{\partial}{\partial\tau} = \left[\frac{\partial\tau}{\partial\tau_0}\right]^{-1}\frac{\partial}{\partial\tau_0} = \frac{1}{\mathcal{F}(\tau,p)}\frac{\partial}{\partial\tau_0}, \tag{C-4}$$

we obtain

$$R_\tau(\tau,p) = \frac{1}{\mathcal{F}(\tau,p)}\frac{\partial R}{\partial \tau_0} = \frac{\mathcal{F}'(\tau,p)}{\mathcal{F}(\tau,p)}\,, \tag{C-5}$$

$$Q_\tau(\tau,p) = \frac{1}{\mathcal{F}(\tau,p)}\frac{\partial Q}{\partial \tau_0} = \frac{\mathcal{F}''(\tau,p)}{\mathcal{F}(\tau,p)}\,. \tag{C-6}$$

Solving equations C-5 and C-6 for $\hat{V}_N$ and $\hat{V}_H$ leads to the *stripping equations* 24 and 25 in the main text. Alternatively, if we replace the τ derivative of the curvature (equation C-4) with the squared derivative of the zero-slope traveltime $\tau^2_{0,\tau}$ (equation C-2) and solve again for $\hat{V}_N$ and $\hat{V}_H$, we obtain *Fowler's equations* 27 and 28 in the main text.

Note that no approximations were made here, other than Alkhalifah's *acoustic approximation* in equation 7. In the case of isotropic or elliptical anisotropy ($\hat{V}_N = \hat{V}_H$), one can just solve equation C-5 for $\hat{V}_N$ obtaining equation 23 in the main text.